



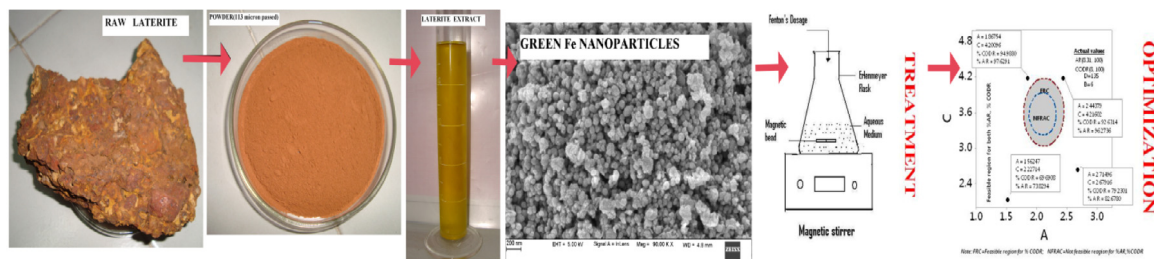
Synthesis of Green Iron Nanoparticles using Laterite and their application as a Fenton-like catalyst for the degradation of herbicide Ametryn in water

Sanjeev Sangami*, Basavaraju Manu

Department of Civil Engineering, National Institute of Technology Karnataka, Surathkal, P.O. Srinivasa nagar, Mangalore-575025 (D.K), India



GRAPHICAL ABSTRACT



HIGHLIGHTS

- Laterite based iron nanoparticles were synthesized using eucalyptus leaf extracts.
- Synthesized iron nanoparticles were applied as a heterogeneous Fenton's catalyst.
- Response surface methodology was proposed for the design of experiments.
- Reaction kinetics indicate that the oxidative degradation of ametryn is very fast.

ARTICLE INFO

Article history:

Received 3 February 2017
Received in revised form 2 June 2017
Accepted 24 June 2017
Available online 11 July 2017

Keywords:

Green synthesis
Laterite
Ametryn

ABSTRACT

The Fe nanoparticles were synthesized using eucalyptus leaf extracts. The low cost and locally available laterite was used as a source of iron rather than using iron salts (Ferrous sulfate, Ferric chloride etc.). The raw laterite particles (RLPs) and synthesized green iron nanoparticles (LGFeNPs) were characterized using FESEM-EDX, XRD, FTIR and BET techniques. The obtained results confirm that 20–70 nm of spherical iron particles were formed with surface area of $36.62 \text{ m}^2/\text{g}$. Later, the LGFeNPs were applied as a Fenton-like catalyst for the degradation ametryn in aqueous medium. The effect of variables ($\text{H}_2\text{O}_2/\text{COD}$ (1–3.25), $\text{H}_2\text{O}_2/\text{Fe}$ (2–10), pH (2–5) and reaction time (30–240)) involved in the treatment process was studied on two responses (COD and ametryn removal efficiency) using the

* Corresponding author.

E-mail addresses: sanjeevenv08@gmail.com (S. Sangami), bmanu@nitk.ac.in (B. Manu).

Fenton-like process
Response surface methodology
Eucalyptus leaf extract

response surface methodology. The optimum values were found to be 2.125, 6, 3.5 and 135 min for H₂O₂/COD, H₂O₂/Fe, pH and reaction time respectively with H₂O₂ dosage of 17 mg/L and 2.83 mg/L of GFeNPs. The analysis of variance (ANOVA) results proved that, the obtained results were satisfactory with predicted values. Compared with chemical (NaBH₄ reduction) and green synthesis using iron salts as a precursor, the laterite based green synthesis proved to be more effective in degradation of ametryn with faster reaction kinetics.

© 2017 Elsevier B.V. All rights reserved.

1. Introduction

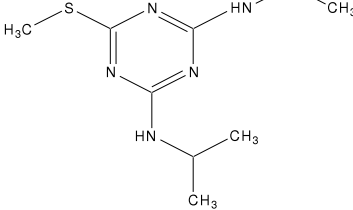
Now a day's water contamination due to the agriculture runoff water containing herbicides is a major concern in drinking water. Ametryn (2-ethylamino-4-(isopropylamino)-6-(methylthio)-s-triazine) is a selective type of herbicide used to kill unwanted plants (broad leaf and grass weeds) from the farmland, waste land, industrial sites, railway embankments and gardens. This is mainly applied to maize and sugar cane field (Sandoval-Carrasco et al., 2013) and only 0.1% is utilized by the targeted plants, major portion retained in the soil itself (Jiang et al., 2008). Due to its high leaching potential and less adsorption by the soil colloids (Kasozi et al., 2012), it is most commonly observed in both surface water and ground water (Laabs et al., 2002; Kolpin et al., 1998). It is also said that the herbicides are the most common pesticides that are detected in water body (Catalkaya and Kargi, 2009) and traces of these herbicides are detected in sugarcane juice in Brazil (Zuin et al., 2006). The ametryn is phototoxic in nature and it moderately affects to fish, highly toxic crustaceans and mollusks, even at lower concentration (Briggs, 1992). Due to its carcinogenicity, creates a lot of potential risks to human beings. Hence, various treatment methods like chlorine dioxide (Lopez et al., 1997), aqueous chlorine (Xu et al., 2009), nanofiltration and reverse osmosis (Shurvel et al., 2014) are adopted to degrade the ametryn from water. However, reverse osmosis and nanofiltration processes require high initial and maintenance costs (Davis, 2007). To overcome all these limitations the Fenton's type of AOPs (advanced oxidation processes) are successfully applied to remove various herbicides in water. It is the mixture of Fe²⁺ and H₂O₂, capable to degrade all types of herbicides by generating highly reactive •OH radical (Arnold et al., 1995; Wang and Lemley, 2001) given in Eq. (1).



However, it is seen that the homogeneous Fenton's process generates high iron sludge and adds extra sulfates from FeSO₄. Therefore, the heterogeneous Fenton-like processes e.g. nano zero valent iron (nZVI) (Xu and Wang, 2011), iron supported clays (Hassan and Hameed, 2011), goethite (α -FeOOH) (Ortiz de la Plata et al., 2010) and Fe₃O₄ (Zhang et al., 2009) have been successfully applied. It is known fact that, the nano size particles have more surface area and reactivity, which helps in easy removal of more toxic chemicals from water (Shahwan et al., 2011). Now a days the iron nanoparticles are synthesized by using sodium borohydride as reducing agent (Xu and Wang, 2011) and co-precipitation of Fe²⁺ and Fe³⁺ (Xu and Wang, 2012) are more popular. However, these methods involve many disadvantages like stability, toxic nature of sodium borohydride, corrosive, an agglomeration of particles, the use of many organic solvents like methanol and are more expensive towards large scale field applications (Chen et al., 2013; Huang et al., 2014). Therefore, recently green syntheses of iron nanoparticles (GFeNPs) using plant extracts have been developed. Many researchers are successfully synthesized GFeNPs and applied as a Fenton's like catalyst to degrade various pollutants, with higher removal efficiency (Shahwan et al., 2011; Kuang et al., 2013). The leaf extract contains polyphenols/caffeine, which acts as a both reducing and capping agent, provides the better platform for the synthesis. All these methods are based on the reduction of Fe²⁺ (ferrous sulfate) or Fe³⁺ (ferric chloride) salts as precursors, lead to the addition of large amounts sulfates and chlorides in the treatment process. To solve this problem, the efforts are made to synthesize iron nanoparticles from locally available laterite from sustainable leaf extracts.

Laterite main composition is iron, aluminum, silicon oxides and Ti, Mg, Mn, Ca, K, Na in small traces (Gualtieri et al., 2015). Moreover, main privileges of laterite are: abundance, low cost, thermally stable, no toxicity in the environment and a proper alternative to the traditional iron. With all these advantages, few researchers were studied the natural laterite as Fenton's catalyst for the removal of sodium azide (Khataee and Pakdehi, 2014), azo dye (Khataee et al., 2015) and paracetamol (Manu and Mahamood, 2011). Since the removal efficiency of pharmaceuticals with iron extracted from a laterite is less compared to ferrous sulfate and hence this can be improved by producing the GFeNPs from natural laterite. In our present study the eucalyptus leaf extracts are preferred, which are non-toxic, biodegradable and contains high amount of polyphenols. The leaves are byproducts of timber and paper mill industry and are considered as a waste except in some cases, the leaves are used for the extraction of oils (medicinal value) (Chen et al., 2014). Recently few researchers were successfully produced the FeNPs from eucalyptus leaves and are applied for the removal of many of the contaminants like nitrate (Wang et al., 2014a), Cr (VI) (Madhavi et al., 2013) and eutrophic wastewater (Wang et al., 2014b). In the present study, the RSM (response surface methodology) was preferred for the design of experiments and it has been successfully applied in the literature related to the removal of Cr⁶⁺ from the green synthesized nano zero valent iron (Yirsaw et al., 2016). Therefore, the main objective is to synthesize the GFeNPs using laterite and apply as a Fenton-like catalyst to degrade the ametryn from aqueous solution using response surface methodology.

Table 1
Physical and chemical properties of Ametryn.

Properties	Ametryn
Structure	
Synonym	2-ethylamino-4-(isopropylamino)-6-(methylthio)-s-triazine
Appearance	White powder
M.W	227.33 g/mol
Chemical formula	C ₉ H ₁₇ N ₅ S
Water solubility (mg/L)	209 at 25 °C
M.P and B.P	84–85 °C and 337 °C
Density (g/cc)	1.18
Adsorption coefficient (<i>K</i> _{oc})	3.45
Leaching potential in soil	6.9
Half life in aerobic soil	53.2 days

2. Materials and methods

2.1. Materials

The Ametryn was purchased from Sigma Aldrich (99% pure) and the physico-chemical properties are listed in Table 1. The reagents, FAS (ferrous ammonium sulfate), HCl (35%), H₂O₂ (30% w/w), NaOH, potassium iodide, ammonium chloride, mercuric sulfate, potassium dichromate, methyl red indicator, silver sulfate, starch, sodium thiosulfate, ultra pure water and methanol (HPLC grade) were obtained from Merck manufactured in India.

2.2. Extraction of iron from laterite

Raw laterite was collected from NITK campus, Surathkal (Karnataka, India) and powdered with hammer, washed with tap water so that light particles were removed. Then, the remaining particles were air-dried, screened through 105 µm sieve and stored in gray bottles. After that 3 g of soil was taken in 500 ml beaker and 15 ml concentrated HCl was added, heated and evaporated to dryness till all HCl disappears. Again the process is repeated and finally 20 ml of hot distilled water is added and filtered it using Whatman 42 filter paper. The residue on the filter paper was ignited in a muffle furnace at 650 °C. The weight of silicon dioxide (SiO₂) was calculated by subtracting the empty weight of crucible. Then the filtrate was diluted to 250 ml and is considered as a mixture of aluminum, iron oxide (Al₂O₃ + Fe₂O₃) and other traces. After that 50% (125 ml) of the liquid part was used to find out the aluminum and iron oxide and the remaining 125 ml was used to separate iron from the mixture according to the IS-2720 (Part-XXV, 1982). The weight of the Al₂O₃ was calculated by subtracting the mixture of aluminum and iron oxide.

2.3. Green synthesis of iron nanoparticles (GFeNPs) using eucalyptus leaves

50 g of eucalyptus leaves was collected from NITK campus and dust particles were removed with distilled water and dried at 40 °C in oven. Then, 15 g of dry leaves were boiled (80 °C) in 250 ml of de-ionized water for about 60 min and vacuum filtered with whatman filter paper no 42 and there after the extracts were stored below 4 °C according the Please check the following cross-citation, and correct if necessary. procedure (Wang et al., 2014a, b). Laterite green iron nanoparticles (LGFeNPs) were prepared by mixing 5.5 g/L of laterite extracted iron with eucalyptus leaves extract with different volume ratios of 1:1, 2:1, 3:1 and 4:1 at room temperature with magnetic stirrer for about 60 min and thereafter vacuum filtered. The appearance of a black color indicated that production of LGFeNPs. The produced LGFeNPs were dried in vacuum at 50 °C for 12 h and stored in gray bottles.

2.4. Characterization of LGFeNPs

Raw laterite particles (RLPs) (105 µm passed) and LGFeNPs were characterized for particle size and shape (FESEM—Field emission scanning electron microscopy), elemental and mineralogical composition (EDX—X-ray energy-dispersive spectrophotometer and XRD—X-ray diffraction), surface area (BET-Brunauer-Emmett-Teller) and for Functional groups

Table 2
Levels of the parameters studied in the CCD.

Factor	Name	Low(−1)	Middle(0)	High(+1)
$A(X_1)$	H_2O_2 /COD	1	2.125	3.25
$B(X_2)$	H_2O_2 /Fe	2	6	10
$C(X_3)$	pH	2	3.5	5
$D(X_4)$	Time (min)	30	135	240

(FTIR-Fourier transform infrared spectroscopy). Smart sorb 92 instrument was used to find out the surface area and pore volume of the particles by BET and Barrett-Joyner-Halenda (BJH) methods respectively. FESEM consists of Carl Zeiss Gemini column, Oxford instruments EDX with Gold sputtering unit. The images are recorded with different magnifications at 5.00 kV voltage. Rigaku Miniflex 600 XRD was used to study the diffraction pattern with mineralogical composition Cu K_α radiation ($\lambda = 1.54 \text{ \AA}$), 40 kV voltage, 15 mA current, with a scanning rate of 1° per min and 2θ range from 10 to 90°. Bruker (Alpha) FTIR having ZnSe optics was used and the KBr (potassium bromide) powder was mixed with particles in the ratio of 5:1 (KBr: sample) and pellets are formed using hydraulic jack, after that the sample was scanned with a wave number range of 375–4000 cm⁻¹.

2.5. Experimental methodology

The working standard solutions of 0.05–0.25 mM were prepared from 0.5 mM ametryn stock solution using ultra pure water. All the standards were analyzed by high performance liquid chromatography (HPLC) and calibration curve was prepared. The degradation studies were initiated by selecting the 0.02 mM (4.54 ppm) as initial concentration, which is near to the actual agriculture runoff water characteristics collected from the study area (0.5 acres of sugarcane field) at Veerapur, Belgaum district in Karnataka state (Latitude: 15°41'27.64"N; Longitude: 74°39'9.11"E) and it was found to be 3.4 ppm.

The batch experiments were conducted in 500 ml Erlenmeyer flask with sample size of 250 ml at room temperatures (29–31 °C) and atmospheric pressure with continuous mixing speed of 210 RPM. Total 26 experiments (runs) were conducted according to the RSM design matrix (Table 2 and 3) and each run was performed in triplicate, the average of the values was considered. The pH (from 2 to 5) of the solution was adjusted with 0.1 N H₂SO₄. After that, the designed dose of iron (0.8–13 mg/L) and H₂O₂ (8–26 mg/L) were added and the Fenton's -like process was initiated. After designed reaction time (30–240 min), the treated sample was dispensed into a glass cylinder and filtered through 0.2μ filter paper. The degradation of ametryn was measured with HPLC calibration curve. The final COD, residual H₂O₂ and final pH were measured. The H₂O₂ interference in COD is corrected according to the literature (Wu and Englehardt, 2012) and the removal efficiency was calculated with Eq. (2). Initially the blank experiment was carryout for 24 h with continuous mixing without adding any reagents and no significant removal was observed.

$$\text{COD removal efficiency} = (\text{COD} - \text{COD}_f) / \text{COD}_i \quad (2)$$

where COD_i is the initial COD (mg/L) and COD_f (mg/L) is its final COD after designed reaction time.

2.6. Analytical procedure

The degradation of ametryn was measured with the HPLC (Agilent 1260) by applying proper conditions like RP-C18 column with size 100 * 4.6 mm, 3.5μ pore size, diode array detector (DAD), column temperature 25 °C, binary pump with flow rate 1 ml/min, mobile phase: methanol: water (58:42), sample volume of 20 μL, and retention time was found to be at 8.8 min. The COD was measured using closed reflux titration method (APHA, 2005) and the pH was measured using a pH meter (Systronics). The λ_{max} (223 nm) value of ametryn was measured using ultra-violet, visible (UV-Vis) double beam spectrophotometer (Systronics, AU-2701). The residual H₂O₂ was measured by iodometric titration.

2.7. Experimental design

The CCD (central composite design) type of RSM was applied to the batch experiments. The CCD contains a full quadratic model equation and it efficiently estimates the first and second-order terms. The CCD consists of three types, central composite circumscribed (CCC), inscribed (CCI) and face centered (CCF) with three types of design points; they are factorial, axial (star points) and center points. In the present study the CCF was selected, with 3 levels (−1, 0, +1) for each factor. The influence of independent factors such as H₂O₂/COD (X_1), H₂O₂/Fe (X_2), pH (X_3) and reaction time (X_4) was studied on two dependent variables (%COD (Y_1) and ametryn removal efficiency (Y_2)). The independent variables were calculated according

Table 3

CCD design matrix.

Run	Independent variables (uncoded and coded)				Fenton's reagent		Actual responses		Predicted responses	
	A (H ₂ O ₂ /COD)	B (H ₂ O ₂ /Fe)	C (P ^H)	D (Time min)	H ₂ O ₂ (mg/L)	Fe (mg/L)	% AR	% CODR	% AR	% CODR
1	2.125(0)	6(0)	3.5(0)	30(-1)	17	2.83	82.35	80	79.639	77.82
2	2.125(0)	10(1)	3.5(0)	135(0)	17	1.7	65	56	64.22	68.33
3	3.25(1)	2(-1)	5(1)	30(-1)	26	13	25.6	24	20.37	20.12
4	2.125(0)	6(0)	3.5(0)	135(0)	17	2.83	100	100	97.21	96.21
5	3.25(1)	10(1)	2(-1)	30(-1)	26	2.6	42.23	36	40.21	26.9
6	2.125(0)	6(0)	2(-1)	135(0)	17	2.83	35.62	28	36.86	28.24
7	3.25(1)	10(1)	5(1)	240(1)	26	2.6	46.23	32	40.5	28.68
8	3.25(1)	2(-1)	5(1)	240(1)	26	13	12.31	16	15.34	17.29
9	2.125(0)	6(0)	3.5(0)	135(0)	17	2.83	100	100	97.21	96.21
10	1(-1)	10(1)	2(-1)	240(1)	8	0.8	35.21	28	34.8	29.12
11	1(-1)	6(0)	3.5(0)	135(0)	8	1.33	28.32	24	33.15	30.55
12	1(-1)	2(-1)	5(1)	30(-1)	8	4	8.31	8	11.09	11.73
13	2.125(0)	6(0)	3.5(0)	240(1)	17	2.83	100	100	100	100
14	1(-1)	10(1)	5(1)	30(-1)	8	0.8	43.62	40	35.8	38.21
15	2.125(0)	6(0)	5(1)	135(0)	17	2.83	45.62	36	48.12	40.12
16	3.25(1)	2(-1)	2(-1)	240(1)	26	13	10.21	8	8.39	8.9
17	3.25(1)	2(-1)	2(-1)	30(-1)	26	13	9.61	8	11.52	9.51
18	3.25(1)	10(1)	2(-1)	240(1)	26	2.6	28.52	24	30.98	23.29
19	1(-1)	2(-1)	2(-1)	240(1)	8	4	12.21	12	10.61	9.73
20	1(-1)	2(-1)	5(1)	240(1)	8	4	12.56	16	13.09	17.12
21	1(-1)	10(1)	5(1)	240(1)	8	0.8	36.52	32	39.86	33.51
22	1(-1)	2(-1)	2(-1)	30(-1)	8	4	14.62	12	10.71	7.34
23	2.125(0)	2(-1)	3.5(0)	135(0)	17	8.5	42.31	44	50.58	46.12
24	1(-1)	10(1)	2(-1)	30(-1)	8	0.8	30.62	28	32.84	29.73
25	3.25(1)	10(1)	5(1)	30(-1)	26	2.6	32.62	24	39.47	29.29
26	3.25(1)	6(0)	3.5(0)	135(0)	26	4.33	21.21	16	25.12	20.12

to Eq. (3) (Zhang et al., 2010), where x_i is the coded notation of the i th factor, X_0 is the value of X_i at the center point and X_D is the step change (difference/2). The interactive effects between dependent and independent variables were expressed as second order polynomial (Eq. (4)).

$$x_i = ((X_i - X_0) / X_D) \dots i = 1, 2, 3 \dots k \quad (3)$$

$$Y = b_0 + \sum_{i=1}^k b_i X_i + \sum_{i=1}^k b_{ii} X_i^2 + \sum_{i=1}^k \sum_{j=1}^k b_{ij} X_i X_j \quad (4)$$

where Y is the response and X_i, X_j are considered as control factors (X_1, X_2, X_3, X_4) and for convenience, all these variables are assigned as A, B, C and D respectively. The b_0 (constant or intercept), b_i (linear term), b_{ii} (quadratic term) and b_{ij} (second order terms) are the coefficients and k is the number of control variables. Total 26 experiments (N) were conducted according to Eq. (5) and the center point is repeated two times for the consistency of the results. The response surface analysis was performed using Minitab software

$$\begin{aligned} N &= \text{factorial Points}(2^k) + \text{axial points}(2 * k) + \text{center points} \\ &= 2^4 + (2 * 4) + 2 = 26 \end{aligned} \quad (5)$$

where n is the number of center points.

In Fenton-like process, the H₂O₂ dosage was decided based on theoretical oxidant required to degrade the ametryn in aqueous solution. Therefore, the COD value of the compound was taken as a reference and the center value of H₂O₂/COD ratio was selected as 2.125, in which the maximum number of •OH radicals are produced (Kim et al., 1997) and the value is near to 2.15 in the previous literature (Kavitha and Palanivelu, 2004). Hence, H₂O₂/COD ratios were selected as 1, 2.125 and 3.25. In many of the literatures, iron dosage was reported as 11.2–28 mg/L (Wang et al., 2016), 10–1000 mg/L (Zhang et al., 2017) and 10 mg/L (Ambika et al., 2016). It was also evident that, this ratio was depending on the type and nature of the compound (Mater et al., 2007). Here, the experiment was started with lower doses of iron (0.8–13 mg/L).

It was proved that, the Fenton's process works in acidic pH from 2 to 5 (Wang et al., 2016; Kuang et al., 2013), 3 to 6 (Ambika et al., 2016; Zhang et al., 2017) and hence, the pH values were considered as 2, 3.5 and 5. The range of reaction time was selected as 30–240 by considering the evidences from other researchers as 0–200 min (Kuang et al., 2013), 0–240 min (Ambika et al., 2016) and 0–45 min (Zhang et al., 2017). All these values are listed in Tables 2 and 3. ANOVA (analysis of variance) was applied to interpret the complex relationship between independent and dependent variables. The coefficient of determination (R^2), Fisher's test (F -test) and the probability (P) value at its 95% confidence level were used to investigate the performance of the second order polynomial equation.

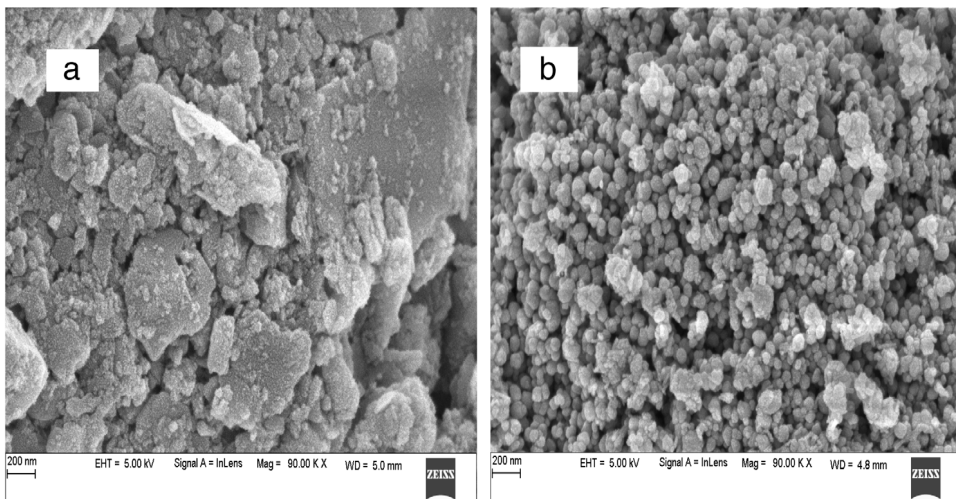


Fig. 1. FESEM images of (a) RLPs (b) LGFeNPs.

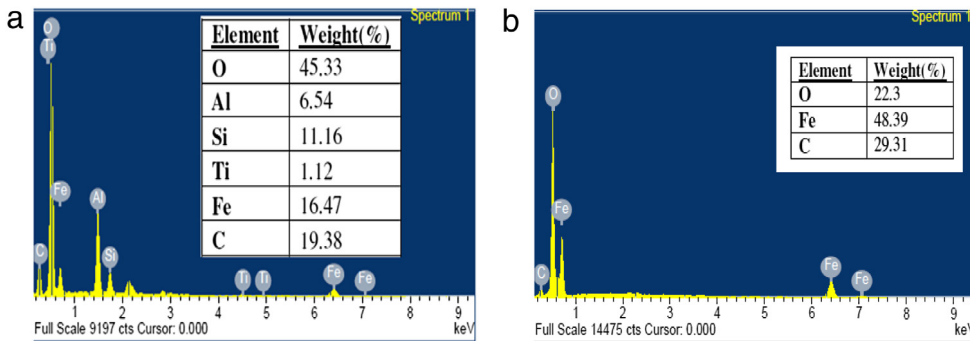


Fig. 2. EDS spectra of (a) RLPs (b) LGFeNPs.

3. Results and discussion

3.1. Characterization

According to the BET analysis, it is seen that surface area and pore volume RLPs are $23.18 \text{ m}^2/\text{g}$, $0.0091 \text{ cm}^3/\text{g}$ and for LGFeNPs $36.62 \text{ m}^2/\text{g}$, $0.0394 \text{ cm}^3/\text{g}$ respectively. With these results it can be concluded that LGFeNPs shows higher surface area and pore volume than RLPs. This may due to the polyphenols present in the eucalyptus leaves, which acts as both reducing agent and capping agent. Fig. 1(a) and (b) shows the FESEM images RLPs and LGFeNPs respectively and it is observed that there is a formation of spherical iron nanoparticles of size 20–70 nm (Fig. 1(b)). The EDX analysis of RLPs (Fig. 2(a)) shows the peaks of C (19.38%), O (45.33%), Si (11.16%), Al (6.54%), Fe (16.47%) and along with a small traces of Ti (1.12%). This proves that there is existence of major portions of Fe_2O_3 , Al_2O_3 and SiO_2 . The Fig. 2(b) shows the EDX spectrum of LGFeNPs with peaks of C (32.31%), O (12.07%), K (7.23%) and Fe (48.39%). The C element is mainly from the polyphenol content in the leaves and it was also observed that there is no Si, Al and Ti were present in LGFeNPs and it is clear that the 100% iron was extracted from laterite.

Fig. 3(a) shows the XRD pattern of RLPs, where the peaks at $2\theta = 19.23, 62.34$ corresponds to the SiO_2 , and peaks at $2\theta = 25.29, 67.82$ represents Fe_2O_3 . The other peaks at 36.35, 64.21, 72.85 are due to the Al_2O_3 and the peak at 34.66 is FeO (ICDD database). Whereas Fig. 3(b) shows the XRD pattern of LGFeNPs in which, the peaks at 17.88, 27.21, 34 and 45.25 corresponds to the polyphenols (Njagi et al., 2011), megahemite ($\gamma\text{-Fe}_2\text{O}_3$), magnetite (Fe_3O_4) and zero valent iron (Fe^0) respectively. The peaks at 24.21, 38.53 represents the iron hydroxides and the peaks at 62.81, 63.59 represents the hematite (Fe_2O_3) respectively (Shahwan et al., 2011; Hoag et al., 2009; Khataee and Pakdehi, 2014).

In FTIR analysis (Fig. 4(a)) the existence of Al-O-H is near to 3670 cm^{-1} and transmittance band between 3680 and 3400 cm^{-1} were the OH group of Si, Al and Fe. The presence of H-O-H on the surface of laterite is near to 1637 cm^{-1} and strong stretching vibration at 1026 cm^{-1} represents the Si-O. The 915, 766, 546 and 446 cm^{-1} indicate the presence of

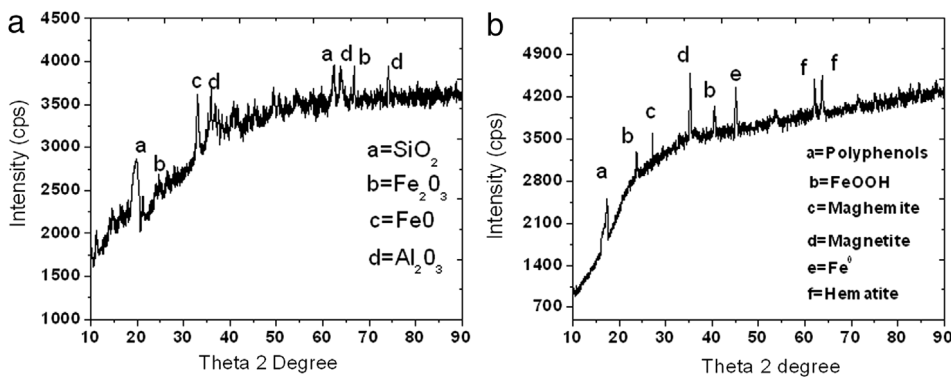


Fig. 3. XRD patterns of (a) RLPs (b) LGFeNPs.

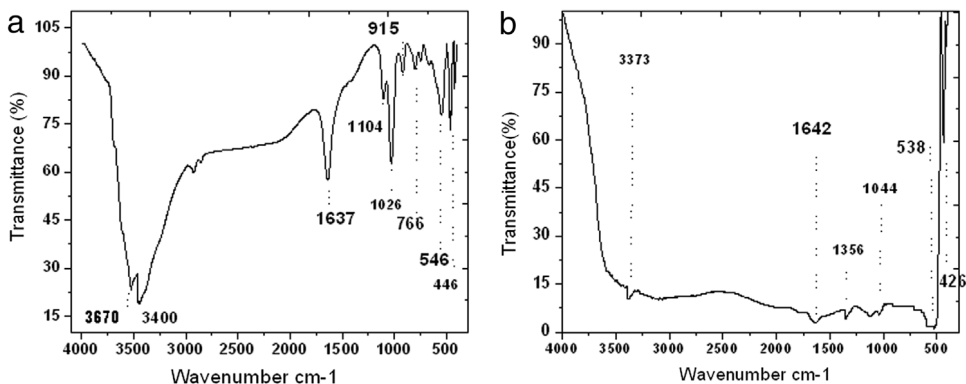


Fig. 4. FTIR spectra of (a) RLPs (b) LGFeNPs.

$\text{Al}-\text{OH}$, cristobalite, Fe_2O_3 and $\text{Fe}-\text{O}$ respectively (Maiti et al., 2010). Fig. 4(b) represents the FTIR spectra of LGFeNPs, in which the wave numbers 3373, 1642, 1356, 1044, 538 and 426 cm^{-1} represents the presence of OH, C=C (polyphenols), C=N (aromatic amines), C-N (aliphatic amines), Fe-O(Fe_3O_4) and Fe-O(Fe_2O_3) (Kumar et al., 2013) respectively. The bands at 538 and 426 cm^{-1} confirms the formation of LGFeNPs and later these particles were oxidized to form iron oxides.

3.2. Degradation studies and statistical analysis

The degradation studies were performed according to the design matrix (Table 3) and second order quadratic equations for both the responses % COD removal efficiency (% CODR) and % ametryn removal efficiency (% AR) were obtained (Eqs. (6) and (7)). Both equations involve one constant term, four first order terms (linear) (A , B , C and D), four second order terms (quadratic) ($A * A$, $B * B$, $C * C$ and $D * D$) and six interaction effects ($A * B$, $A * C$, $A * D$, $B * C$, $B * D$ and $C * D$).

$$\begin{aligned} \% \text{CODR}(Y_1) = & 70.34 - 0.67 A + 8.44 B + 2.44 C + 0.44 D - 40.5 A * A - 10.5 B * B - 28.5 C * C \\ & + 29.5 D * D - 1.25 A * B + 0.25 A * C - 0.75 A * D - 0.75 B * C - 0.75 B * D + 0.75 C * D \end{aligned} \quad (6)$$

$$\begin{aligned} \% \text{AR}(Y_2) = & 73.75 + 0.36 A + 11.82 B + 2.47 C + 0.23 D - 40.23 A * A - 11.34 B * B - 24.36 C * C \\ & + 26.18 D * D - 0.4 A * B + 1.12 A * C - 0.76 A * D + 0.64 B * C + 0.51 B * D + 0.53 C * D. \end{aligned} \quad (7)$$

In both equations the intercept values, and coefficients of B , C , D , $D * D$, $A * C$, $C * D$ are showing a positive effect. Also in Eq. (7) $B * C$ and $B * D$ are having a positive effect on the response and the coefficient of D^2 has the highest positive values of 29.5 and 26.18, implies that the reaction time is the more influencing parameter on the both responses. According to the ANOVA results (Tables 4 and 5), the most significant factors are B , A^2 , C^2 , D^2 and A^2 , C^2 , D^2 for Y_2 and Y_1 respectively with the P value < 0.05 . The F values (relation between the mean square and the residual error of the model) were determined to find out the best fit of the model to the observed data and values were observed to be 5.34 and 4.34 for Y_2 and Y_1 respectively. These values are greater than tabular $F_{0.05(14,11)}$ value of 2.74 and hence, it is confirmed as the most significant model. The coefficient of determination (R^2) is also calculated to know the variation between the actual responses and fits.

Table 4

Analysis of variance for % AR.

Source	DF	Adj SS	Adj MS	F-value	P-value > F
Model	14	17 499.5	1249.96	5.34	0.004
Linear	4	2630.0	657.51	2.81	0.079
A	1	2.4	2.38	0.01	0.921
B	1	2516.5	2516.48	10.74	0.007
C	1	110.2	110.21	0.47	0.507
D	1	1.0	0.98	0.00	0.950
Square	4	14 822.6	3705.64	15.82	0.000
A * A	1	4145.6	4145.61	17.70	0.001
B * B	1	329.6	329.55	1.41	0.261
C * C	1	1522.1	1522.06	6.50	0.027
D * D	1	1754.8	1754.76	7.49	0.019
2-way interaction	6	46.9	7.82	0.03	1.000
A * B	1	2.6	2.56	0.01	0.919
A * C	1	19.9	19.89	0.08	0.776
A * D	1	9.2	9.18	0.04	0.847
B * C	1	6.6	6.60	0.03	0.870
B * D	1	4.2	4.24	0.02	0.895
C * D	1	4.4	4.41	0.02	0.893
Residual	11	2576.3	234.21		
Lack-of-fit	10	2576.3	257.63	1.6	
Pure error	1	0.0	0.00		
Total	25	20 075.8			

Note: $R^2 = 92.34\%$; $R_{adj}^2 = 91.36\%$; Standard deviation (S.D) = 2.21; Coefficient of variation (C.V) = 9.66%; Adequate precision (A.P) = 18.03.**Table 5**

Analysis of variance for % CODR.

Source	DF	Adj SS	Adj MS	F-value	P-value > F
Model	14	17107.7	1221.98	4.34	0.010
Linear	4	1402.7	350.67	1.24	0.348
A	1	8.0	8.00	0.03	0.869
B	1	1283.6	1283.56	4.56	0.056
C	1	107.6	107.56	0.38	0.549
D	1	3.6	3.56	0.01	0.913
Square	4	15643.0	3910.76	13.88	0.000
A * A	1	4191.8	4191.75	14.88	0.003
B * B	1	280.0	280.05	0.99	0.340
C * C	1	2073.9	2073.90	7.36	0.020
D * D	1	2235.2	2235.17	7.93	0.017
2-way interaction	6	62.0	10.33	0.04	1.000
A * B	1	25.0	25.00	0.09	0.771
A * C	1	1.0	1.00	0.00	0.954
A * D	1	9.0	9.00	0.03	0.861
B * C	1	9.0	9.00	0.03	0.861
B * D	1	9.0	9.00	0.03	0.861
C * D	1	9.0	9.00	0.03	0.861
Residual	11	3099.7	281.79		
Lack-of-fit	10	3099.7	309.97	0.8	
Pure error	1	0.0	0.00		
Total	25	20207.4			

Note: $R^2 = 95.4\%$; $R_{adj}^2 = 92.30\%$; Standard deviation (S.D) = 2.26; Coefficient of variation (CV) = 8.62%; Adequate precision (AP) = 17.17.

The R^2 and R_{adj}^2 values are found to be 92.34%, 95.46% and 91.36%, 92.3% for Y_2 and Y_1 respectively. With these results, it is proved that R^2 and R_{adj}^2 are close to each other, $R^2 > 80\%$ and $R_{adj}^2 < R^2$. From Tables 4 and 5 it is observed, the lack of fit and the residual error are showing the similar values 2576.3 and 3099.7 with pure error zero for both ametryn and COD removal respectively. The lack of fit F values are 1.6% and 0.8% for Y_2 and Y_1 respectively and these values are due to the noise in the responses (Im et al., 2012). All these results confirm the good agreement between the predicted and experimental values.

The standard deviation (S.D = how many values in responses are differing from a mean value), coefficient of variation (C.V = It is a percentage ratio of standard error to the mean value of the response) and adequate precision (A.P = It is the ratio of the predicted response to its error) of both responses were determined. The S.D values are very less and are 2.21 and 2.26 for Y_2 and Y_1 respectively. The C.V values are 9.66 (Y_2), 8.62 (Y_1), which are less than 10% (Beg et al., 2003) and A.P values are 18.03 (Y_2), 17.17 (Y_1) and the desired value is 4 or >4 (Zinatizadeh et al., 2006). Hence, the results obtained are reliable. The normal probability distribution of data points is plotted against the residuals in Fig. 5(a) (b) and the points are distributed near the straight line, which confirms that the results are best fit with the predicted values.

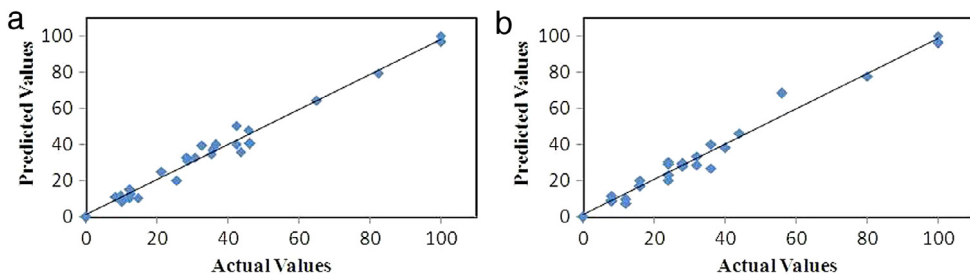


Fig. 5. Plot of predicted versus actual values for both responses (a) % CODR (b) % AR.

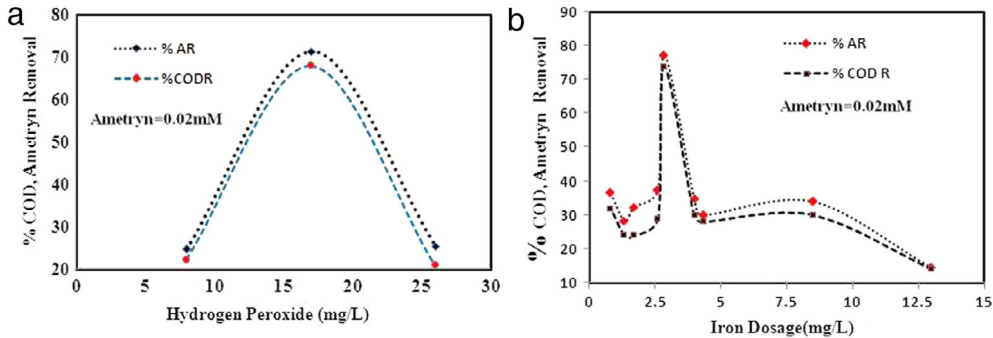


Fig. 6. Removal efficiency vs. (a) dosage of H₂O₂ (b) dosage of iron.

3.3. Effect of H₂O₂ and Fe on the responses

The effect of H₂O₂ on the removal efficiency was studied based on the H₂O₂/COD ratio (1, 2.125 and 3.25). It was observed that, as the ratio is decreased to 1 or increased to 3.25 from a center value of 2.125, less removal was observed. It indicates that, the more number of hydroxyl radicals are produced in the ratio of 2.125 (Kim et al., 1997) and thereby increasing the removal efficiency. Based on this, the dosage of H₂O₂ was varied from 8 to 26 mg/L (Table 3). Usually, it is seen that, increase in the H₂O₂, increases the degradation of pollutants by generating the more hydroxyl radicals (Pignatello, 1992). However, when the concentration of H₂O₂ was 26 mg/L, the removal efficiency (both Y₂ and Y₁) was <45% and may be this is due to the, addition the excess amount of H₂O₂, decreases the further production of •OH radicals (Eq. (8)) (scavenging effect) (Masomboon et al., 2009). Also, when the dosage of H₂O₂ was 8 mg/L, the removal efficiency was <43%, because insufficient H₂O₂ for •OH radical production. Hence, 17 mg/L of H₂O₂ with H₂O₂/COD ratio of 2.125 was finally considered, in which 100% removal was observed (Fig. 6(a)).



The dosage of iron (LGFeNPs) is another important factor in Fenton-like process which exploits the rate of reaction and is as important as H₂O₂. The selection of iron dosage depends on the suitable values of H₂O₂/Fe ratio (2, 6 and 10). Based on this, the effect of iron (0.8–13 mg/L) was studied in the degradation process. At high iron doses of 13, 8.5, 4.33 and 4 mg/L the less ametryn removal (<45%) was achieved and this may due to the agglomeration of LGFeNPs (Garrido-Ramírez et al., 2010) and more number of Fe²⁺ ions scavenged the already produced •OH radicals shown in Eq. (9) (Pignatello, 1992). Furthermore, when iron dose was <2.83 mg/L, there is a less production of Fe²⁺ ions (a reaction between Fe⁰ and oxidant) and after that the H₂O₂ was going to react with already produced •OH radicals to form a •OOH radical (Eqs. (10) and (11)) and the formed •OOH radicals were having less oxidation capacity than •OH radicals (Masomboon et al., 2009). Hence, the optimum iron dose of 2.83 mg/L (H₂O₂/Fe = 6) was finally considered (Fig. 6(b)).



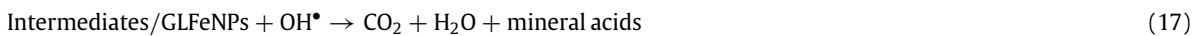
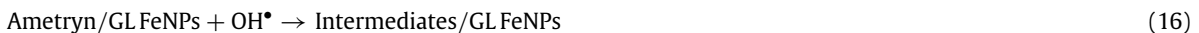
3.4. Effect of pH on the responses

The heterogeneous (laterite) and homogeneous (FeSO₄·7H₂O, FeCl₃) Fenton processes were influenced by the pH and in the present study the pH varied from 2 to 5. In case of run 6 (pH 2, % AR and % CODR < 36) and run 15 (pH 5, % AR and

% CODR < 46), the less ametryn removal was achieved even though of optimum iron (2.83 mg/L) and H₂O₂ (17 mg/L). It signifies that, relative increase (10%) in the ametryn removal was achieved at pH 5 than pH 2. Similar kind of results were observed in the literatures related to the heterogeneous Fenton process for removal of many of the contaminants such as 17 β -estradiol (α -FeOOH coated resin vs. H₂O₂) with removal efficiencies of 98.2% at pH 3.07 and 86.4% at pH 7.47 (Yaping and Jiangyong, 2008), salicylic acid (H₂O₂ vs. goethite) with removal efficiency from 95% to 45% (pH 6–11). Also few homogeneous Fenton degradation studies were reported that, the removal efficiency was maximum at pH 3 and negligible (<5%) at pH 7 (Zhou et al., 2004; Neppolian et al., 2004). This clearly indicates that, the heterogeneous Fenton process has relatively more advantage towards alkaline pH than acidic pH and this is mainly depends on the surface characteristics and leaching potential of LGFeNPs. The heterogeneous Fenton process proceeds with adsorption of ametryn on to the surface of the iron oxides, iron hydroxides and Fe⁰ (XRD analysis of LGFeNPs) followed by production of the •OH radicals and these radicals reacts with ametryn to form mineralization products. As discussed earlier, at pH 2 less ametryn removal was observed and this may be due to the leaching of iron from iron oxide and hydroxide surfaces. This dissolved iron forms oxyhydroxides, which are more stable with lesser catalytic activity. Similar kind of reaction mechanism was observed, when the heterogeneous process (dissolved iron, 86.4% removal E2 at pH 7.47) and homogeneous Fenton processes (Fe³⁺, 46.3% removal E2 at pH 7.47) were compared (Yaping and Jiangyong, 2008). Chou et al. (2001) also reported that, at pH < 4 more leaching of iron was observed from the FeOOH. On the other hand, at pH 5, may be it favors the adsorption of ametryn on to the surface of iron particles and after that, deactivation of a Fe²⁺ ions by forming ferric hydroxide complexes, which reduces the generation of •OH radicals (Lucas and Peres, 2006) and stops further reactions. Finally from Table 3, it was observed that at pH 3.5 (4, 9 and 13), 100% removal (both responses) was achieved and may be at this stage (pH = 3.5), no leaching of iron was observed and fully recycling of iron occurred directly on to the catalyst surface. Hence, the optimum pH of 3.5 was maintained in the treatment process.

3.5. Effect of reaction time on the responses

The reaction time (*D*) is also having a significant influence in generating the •OH radicals and was varied from 30 to 240 min. In case of run 1 at 30 min (pH = 3.5, Fe = 2.83 mg/L, H₂O₂ = 17 mg/L), the reaction was faster and 83% of removal was achieved. With similar experimental conditions the reaction process was continued (runs 4, 9 and 13) and it was observed that 100% removal was achieved in 135 min. The possible degradation pathway consists of adsorption, generation of OH radicals and mineralization processes. The XRD analysis report shows that, there is existence of Fe₂O₃, Fe₃O₄ and Fe⁰ and at the initial stages (30 min), the ametryn adsorbs on the surface of the LGFeNPs and later the oxidant (H₂O₂) reacts with Fe⁰ and converts to Fe²⁺ and also in parallel, the conversion of Fe²⁺/Fe³⁺ from Fe₂O₃/Fe₃O₄ was observed by reacting with H⁺ ions (optimum pH of the solution is 3.5). After that, the hydroxyl radicals were produced (a reaction between oxidant and Fe²⁺) (Eqs. (12)–(15)) (Xue et al., 2009; Garrido-Ramírez et al., 2010; Kuang et al., 2013). These OH radicals attack the ametryn on the LGFeNPs surface and mineralize the process (CO₂, H₂O and mineral acids) (Eqs. (16)–(17)). After 30 min, the reaction was slowly reduced and this may be due to the production of hydroperoxyl radicals (HO₂[•]) (Eqs. (18)–(19)) (Rusevova et al., 2012). However, in case of the runs (3, 5, 12, 14, 17, 22, 24, and 25) at 30 min, less removal (8%–46%) was achieved, which indicates that the efficiency is also depends on the dosage of iron, oxidant and pH.



To understand the reaction kinetics involved in the whole treatment process, the experiments were conducted in optimal conditions (Fe = 2.83 mg/L, H₂O₂ = 17 mg/L and pH = 3.5) and obtained results were plotted in Fig. 7(a) (ln C_t/C₀ and ln COD_t/COD₀ vs. time). It was clear that, the linear relationship was established with R² (correlation coefficient) value of >0.9 and hence, the experimental data was best fit with the pseudo-first order kinetic model (Eqs. (20)–(21)).

$$\ln C_t/C_0 = -K_1 t \quad (20)$$

$$\ln \text{COD}_t/\text{COD}_0 = -K_2 t \quad (21)$$

where C_t and COD_t are concentration and COD at the time *t* min and C₀ and COD₀ concentration and COD at time 0 min. The K₁ and K₂ are the slopes of the decay curves and are considered to be 1st order rate constants in min⁻¹. From Fig. 7(a), it was clear that the rate of reaction of % COD removal efficiency (K₂ = 0.024 min⁻¹) was less than the % ametryn removal efficiency (K₁ = 0.033 min⁻¹). This may due to the fact that, the conversion from the ametryn to the intermediates is faster than the

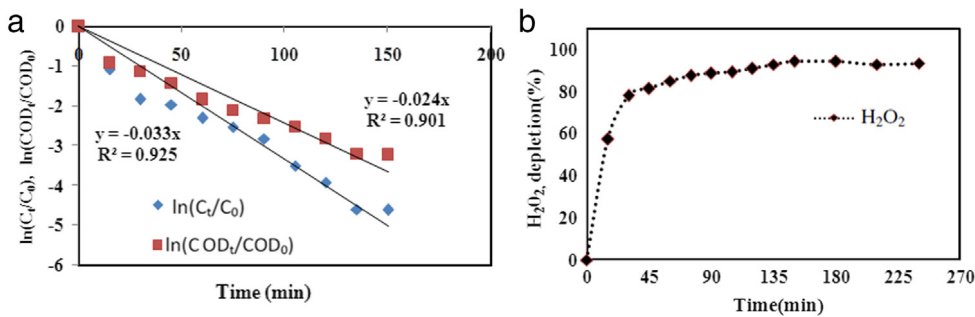


Fig. 7. (a) Residual $\text{COD}_t/\text{COD}_0$, C_t/C_0 with time (b) H_2O_2 depletion vs. time.

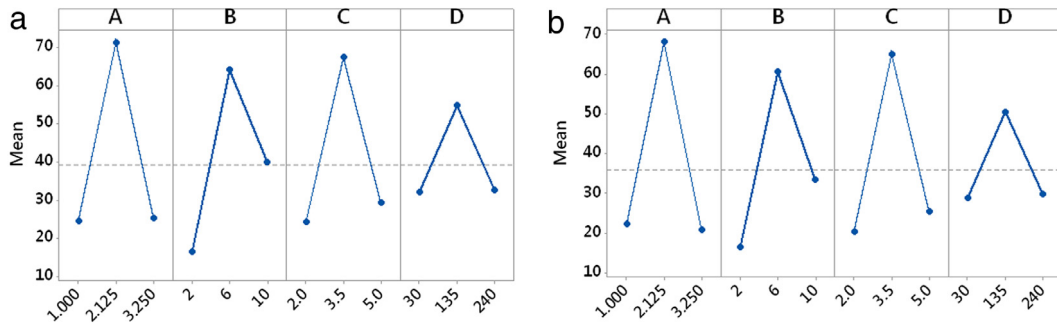


Fig. 8. Main affects plots for both responses (a) % CODR (b) % AR.

intermediates to the mineralization (CO_2 , H_2O and mineral acids). A similar kind of pseudo-first order kinetic models were obtained in other studies also (Swaminathan et al., 2003 ($R^2 = 0.89\text{--}0.99$, $K = 0.01\text{--}0.07 \text{ min}^{-1}$); Kong and Lemley, 2006 ($R^2 = 0.71\text{--}0.97$, $K = 0.04\text{--}0.32 \text{ min}^{-1}$); Zhang et al., 2016 ($R^2 = 0.99\text{--}1$, $K = 0.0022\text{--}0.0046 \text{ min}^{-1}$); Ma et al., 2000 ($R^2 = 0.91\text{--}0.99$, $K = 0.004\text{--}0.06 \text{ min}^{-1}$)). Further, the oxidant decomposition was also monitored (Fig. 7(b)) and it is seen that 100% depletion of H_2O_2 was observed within 90 min. This implies that, the more number of hydroxyl radicals were produced at the initial stages. Finally, from the Fig. 8(a)(b) the optimum values are confirmed as 2.125, 6, 3.5 and 135 for A, B, C and D respectively.

3.6. Optimization and validation

To determine the optimum region or working feasible region the contours are graphically overlaid for both responses (Ahmad et al., 2005) and in this process the desired goal was to maximize the responses Y_1 (% CODR) and Y_2 (% AR). Hence, the boundary values were defined as $Y_1(8, 100)$ and $Y_2(8.31, 100)$ with a reaction time of 135 min. The overlay plot consists of 3 regions, which are separated by circular dotted lines shown in Fig. 9. The shaded portion consists of 2 regions, the middle area is not feasible region for both % AR and % CODR (NFRAC) and other region is feasible for only % CODR (FRC). The remaining unshaded area (optimum region) is feasible for both responses. To validate the obtained results, four sets of additional experiments were carried out by selecting the random values from the unshaded area and are tagged in Fig. 9. The results of those experiments (Run 27, 28, 29 and 30) were listed in Table 6. The standard deviation (<5) coefficient of variation ($<9\%$) and adequate precision (A.P) is greater than 12 and these values are within the prescribed limits ($S.D < 4$, $C.V < 10\%$ and $A.P > 4$). It clearly says that, predicted and experimental values are well fitted.

4. Conclusions

In this study the iron nanoparticles were synthesized from a raw laterite using eucalyptus leaf extract. After that, these nanoparticles were used as a catalyst in Fenton-like process for the oxidation of ametryn in aqueous medium using response surface methodology. Based on the results the following conclusions were drawn.

- (1) With FESEM and BET analysis, it was found that 20–70 nm of spherical particles (GLFeNPs) were formed with surface area of $36.62 \text{ m}^2/\text{g}$.
- (2) The XRD analysis shows that GLFeNPs consists of mainly Fe^0 , Fe_2O_3 , Fe_3O_4 and polyphenols and are confirmed by FTIR analysis.

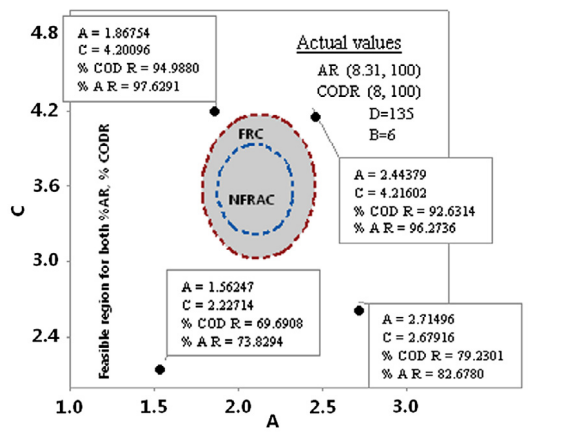


Fig. 9. Contour overlay plot.

Table 6
Optimization of additional experiments.

Run	Independent factors				% CODR ^a		% AR ^b		Error		S.D ^c		C.V ^d		A.P ^e	
	A	B	C	D	Ac ^f	Pr ^g	Ac	Pr	% CODR	% AR	% CODR	% AR	% CODR	% AR	% CODR	% AR
27	1.87	6	4.2	135	92	94.98	92.31	97.62	2.98	5.31	2.11	3.75	3.19	5.59	31.87	18.38
28	2.44	6	4.21	135	88	92.63	93.3	96.97	4.63	3.67	3.27	2.6	5.13	3.86	20.01	26.42
29	1.56	6	2.22	135	64	69.69	71.58	73.82	5.69	2.24	4.02	1.58	8.51	3.08	12.25	32.96
30	2.71	6	2.67	135	76	79.23	78.62	82.6	3.23	3.98	2.28	2.81	4.16	4.94	24.53	20.75

^a % CODR = % COD removal.

^b % AR = % ametryn removal.

^c S.D = Standard deviation.

^d C.V = Coefficient of variation.

^e A.P = Adequate precision.

^f Ac = Actual values.

^g Pr = Predicted values.

- (3) The 100% removal of ametryn was achieved with an optimum value of 2.125 (A), 6 (B), 3.5 (C) and 135 (D) min with iron and H₂O₂ values of 2.83 and 17 mg/L respectively.
- (4) The pseudo-first order kinetic model was successfully established with experimental data having R² (correlation coefficient) value >0.9 for both the responses.
- (5) The S.D, C.V and A.P values were 2.21, 9.66% and 18.03 for % AR respectively and for % CODR, these values are 2.26, 8.62% and 17.17. All these values are within the prescribed limits (S.D < 4, C.V < 10% and A.P > 4). The treatment process was validated by conducting the additional experiments suggested by contour overlay plot, in which the experimental findings were well fitted with the predicted values. Conclusively, synthesis and degradation process was carried out by using locally available laterite, which is cost effective and promising technique for the complete degradation of ametryn in water.

Acknowledgment

The authors are grateful to MHRD Govt. of India (No.33197 /2015/E.III(A) dated 18.02.2015) for Institute fellowship to carry out this research.

References

- Ahmad, A.L., Ismail, S., Bhatia, S., 2005. Optimization of coagulation-flocculation process for palm oil mill effluent using RSM. Environ. Sci. Technol. 39, 2828–2834.
- Ambika, S., Devasena, M., Nambi, I.M., 2016. Synthesis, characterization and performance of high energy ball milled meso-scale zero valent iron in Fenton reaction. J. Environ. Manag. 181, 847–855.
- APHA, AWWA, WPCF (Eds.), 2005. Standard methods for the examination of water and wastewater. Washington DC.
- Arnold, S.M., Hickey, W.J., Harris, R.F., 1995. Degradation of atrazine by Fenton's reagent: Condition optimization and product quantification. Environ. Sci. Technol. 29, 2083–2089.

- Beg, Q., Sahai, V., Gupta, R., 2003. Statistical media optimization and alkaline protease production from *Bacillus mojavensis* in a bioreactor. *Process. Biochem.* 39, 203–209.
- Briggs, S.A., 1992. Basic Guide To Pesticides: Their Characteristics and Hazards. Hemisphere Publishing, Washington DC.
- Catalkaya, E.C., Kargi, F., 2009. Degradation and mineralization of simazine in aqueous solution by ozone/hydrogen peroxide advanced oxidation. *J. Environ. Eng.* 135, 1357–1364.
- Chen, Z., Wang, T., Jin, X., Chen, Z., Megharaj, M., Naidu, R., 2013. Multifunctional kaolinite-supported nanoscale zero-valent iron used for the adsorption and degradation of crystal violet in aqueous solution. *J. Colloid Interface Sci.* 398, 59–66.
- Chen, Y., Wang, J., Ou, Y., Chen, H., Xiao, S., Liu, G., Huang, Q., 2014. Cellular antioxidant activities of polyphenols isolated from Eucalyptus leaves (*Eucalyptus grandis* × *Eucalyptus urophylla* GL9). *J. Funct. Foods* 7, 737–745.
- Chou, S.S., Huang, C.P., Huang, Y.H., 2001. Heterogeneous and homogeneous catalytic oxidation by supported gamma-FeOOH in a fluidized bed reactor: kinetic approach. *Environ. Sci. Technol.* 35 (6), 1247–1251.
- Davis, A.P., 2007. Field performance of bioretention: water quality. *Environ. Eng. Sci.* 24, 1048–1064.
- Garrido-Ramírez, E.G., Theng, B.K.G., Mora, M.L., 2010. Clays and oxide minerals as catalysts and nanocatalysts in Fenton-like reactions—a review. *Appl. Clay Sci.* 47, 182–192.
- Gualtieri, M.L., Romagnoli, M., Pollastri, S., Gualtieri, A.F., 2015. Inorganic polymers from laterite using activation with phosphoric acid and alkaline sodium silicate solution: Mechanical and microstructural properties. *Cem. Concr. Res.* 67, 259–270.
- Hassan, H., Hameed, B.H., 2011. Fe-clay as effective heterogeneous Fenton catalyst for the decolorization of reactive blue 4. *Chem. Eng. J.* 171, 912–918.
- Hoag, G.E., Collins, J.B., Holcomb, J.L., Hoag, J.R., Nadagouda, M.N., Varma, R.S., 2009. Degradation of bromothymol blue by “greener” nano-scale zero-valent iron synthesized using tea polyphenols. *J. Mater. Chem.* 19, 8671–8677.
- <https://law.resource.org/pub/in/bis/S03/is.2720.25.1982.pdf> Indian Standard methods of test for soils IS:2720(Part XXV)-1982.
- Huang, L., Weng, X., Chen, Z., Megharaj, M., Naidu, R., 2014. Synthesis of iron-based nanoparticles using oolong tea extract for the degradation of malachite green. *Spectrochim. Acta. A* 3, 801–804.
- Im, J.-K., Cho, I.-H., Kim, S.-K., Zoh, K.-D., 2012. Optimization of carbamazepine removal in O₃/UV/H₂O₂ system using a response surface methodology with central composite design. *Desalination* 285, 306–314.
- Jiang, L., Huang, J., Liang, L., Zheng, Y.P., Yang, H., 2008. Mobility of prometryne in soil as affected by dissolved organic matter. *J. Agric. Food. Chem.* 56, 11933–11940.
- Kasozzi, G.N., Nkedi-Kizza, P., Li, Y., Zimmerman, A.R., 2012. Sorption of atrazine and ametryn by carbonatic and non-carbonatic soils of varied origin. *Environ. Pollut.* 169, 12–19.
- Kavitha, V., Palanivelu, K., 2004. The role of ferrous ion in Fenton and photo-Fenton processes for the degradation of phenol. *Chemosphere* 55, 1235–1243.
- Khataee, A.R., Pakdehi, S.G., 2014. Removal of sodium azide from aqueous solution by Fenton-like process using natural laterite as a heterogeneous catalyst: Kinetic modeling based on nonlinear regression analysis. *J. Taiwan Inst. Chem. Eng.* 45, 2664–2672.
- Khataee, A., Salahpour, F., Fathinia, M., Seyyedi, B., Vahid, B., 2015. Iron rich laterite soil with mesoporous structure for heterogeneous Fenton-like degradation of an azo dye under visible light. *J. Ind. Eng. Chem.* 26, 129–135.
- Kim, S., Geissen, S., Vogelpohl, A., 1997. Landfill leachate treatment by a photoassisted Fenton reaction. *Water Sci. Technol.* 35, 239–248.
- Kolpin, D.W., Thurman, E.M., Linhart, S.M., 1998. The environmental occurrence of herbicides: the importance of degradates in ground water. *Arch. Environ. Contam. Toxicol.* 35, 385–390.
- Kong, L., Lemley, A.T., 2006. Kinetic modeling of 2, 4-dichlorophenoxyacetic acid (2, 4-D) degradation in soil slurry by anodic Fenton treatment. *J. Agric. Food. Chem.* 54 (11), 3941–3950.
- Kuang, Y., Wang, Q., Chen, Z., Megharaj, M., Naidu, R., 2013. Heterogeneous Fenton-like oxidation of monochlorobenzene using green synthesis of iron nanoparticles. *J. Colloid Interface Sci.* 410, 67–73.
- Kumar, K.M., Mandal, B.K., Kumar, K.S., Reddy, P.S., Sreedhar, B., 2013. Biobased green method to synthesise palladium and iron nanoparticles using Terminalia chebula aqueous extract. *Spectrochim. Acta A* 102, 128–133.
- Laabs, V., Ameling, W., Pinto, A.A., Wantzen, M., Silva, C.J., Zech, W., 2002. Pesticides in surface water, sediment, and rainfall of the northeastern Pantanal basin, Brazil. *J. Environ. Qual.* 31 (5), 1636–1648.
- Lopez, A., Mascolo, G., Tiravanti, G., Passino, R., 1997. Degradation of herbicides (ametryn and isoproturon) during water disinfection by means of two oxidants (hypochlorite and chlorine dioxide). *Water Sci. Technol.* 35, 129–136.
- Lucas, M.S., Peres, J.A., 2006. Decolorization of the azo dye reactive black 5 by Fenton and photo-Fenton oxidation. *Dye. Pigment.* 71, 236–244.
- Ma, Y.S., Huang, S.T., Lin, J.G., 2000. Degradation of 4-nitrophenol using the Fenton process. *Water Sci. Technol.* 42 (3–4), 155–160.
- Madhavi, V., Prasad, T.N.V.K.V., Reddy, A.V.B., Reddy, B.R., Madhavi, G., 2013. Application of phytogenic zerovalent iron nanoparticles in the adsorption of hexavalent chromium. *Spectrochim. Acta Part A* 116, 17–25.
- Maiti, A., Basu, J.K., De, S., 2010. Development of a treated laterite for arsenic adsorption: effects of treatment parameters. *Ind. Eng. Chem. Res.* 49, 4873–4886.
- Manu, B., Mahamood, S., 2011. Enhanced degradation of paracetamol by UV-C supported photo-Fenton process over Fenton oxidation. *Water Sci. Technol.* 64 (12), 2433–2438.
- Masombon, N., Ratanatamskul, C., Lu, M., 2009. Chemical Oxidation of 2,6- imethylaniline in the Fenton Process. *Environ. Sci. Technol.* 43, 8629–8634.
- Mater, L., Rosa, E.V.C., Berto, J., Corrêa, A.X.R., Schwingel, P.R., Radetski, C.M., 2007. A simple methodology to evaluate influence of H₂O₂ and Fe²⁺ concentrations on the mineralization and biodegradability of organic compounds in water and soil contaminated with crude petroleum. *J. Hazard. Mater.* 149, 379–386.
- Nepolian, B., Park, J.S., Choi, H., 2004. Effect of Fenton-like oxidation on enhanced oxidative degradation of para-chlorobenzoic acid by ultrasonic irradiation. *Ultrason. Sonochem.* 11 (5), 273–279.
- Njagi, E.C., Huang, H., Stafford, L., et al., 2011. Biosynthesis of iron and silver nanoparticles at room temperature using aqueous sorghum bran extracts. *Langmuir* 27, 264–271.
- Ortiz de la Plata, G.B., Alfano, O.M., Cassano, A.E., 2010. Decomposition of 2- chlorophenol employing goethite as Fenton catalyst. I. Proposal of a feasible, combined reaction scheme of heterogeneous and homogeneous reactions. *Appl. Catal. B* 95, 1–13.
- Pignatello, J.J., 1992. Dark and photoassisted Fe³⁺ Catalyzed degradation of chlorophenoxy herbicides by hydrogen peroxide. *Environ. Sci. Technol.* 26, 944–951.
- Rusevova, K., Kopinke, F.D., Georgi, A., 2012. Nano-sized magnetic iron oxides as catalysts for heterogeneous Fenton-like reactions—Influence of Fe (II)/Fe (III) ratio on catalytic performance. *J. Hazard. Mater.* 241, 433–440.
- Sandoval-Carrasco, C.A., Ahuatz-Checa, D., Galíndez-Mayer, J., Ruiz-Ordaz, N., Juárez-Ramírez, C., Martínez-Jerónimo, F., 2013. Biodegradation of a mixture of the herbicides ametryn, and 2,4-dichlorophenoxyacetic acid (2,4-D) in a compartmentalized biofilm reactor. *Bioresour. Technol.* 145, 33–36.
- Shahwan, T., AbuSirriah, S., Nairat, M., Boyac, A.E., Ero-glu, T.B., Scott, K.R., et al., 2011. Green synthesis of iron nanoparticles and their application as a Fenton-like catalyst for the degradation of aqueous cationic and anionic dyes. *Chem. Eng. J.* 172, 258–266.
- Shurvel, T., Keir, G., Jegatheesan, V., Shu, L., Farago, L., 2014. Removal of ametryn through nanofiltration and reverse osmosis. *Desalin. Water Treat.* 52, 643–649.

- Swaminathan, K., Sandhya, S., Sophia, A.C., Pachhade, K., Subrahmanyam, Y.V., 2003. Decolorization and degradation of H-acid and other dyes using ferrous-hydrogen peroxide system. *Chemosphere* 50 (5), 619–625.
- Wang, T., Jiajiang, L., Chen, Z., Megharaj, M., Naidu, R., 2014a. Green synthesized iron nanoparticles by green tea and eucalyptus leaves extracts used for removal of nitrate in aqueous solution. *J. Cleaner Prod.* 83, 413–419.
- Wang, T., Jin, X., Chen, Z., Megharaj, M., Naidu, R., 2014b. Green synthesis of Fe nanoparticles using eucalyptus leaf extracts for treatment of eutrophic wastewater. *Sci. Total Environ.* 466–467, 210–213.
- Wang, Q.Q., Lemley, A.T., 2001. Kinetic model and optimization of 2,4-D degradation by anodic Fenton treatment. *Environ. Sci. Technol.* 35, 4509–4514.
- Wang, L., Yang, J., Li, Y., Lv, J., Zou, J., 2016. Removal of chlorpheniramine in a nanoscale zero-valent iron induced heterogeneous Fenton system: Influencing factors and degradation intermediates. *Chem. Eng. J.* 284, 1058–1067.
- Wu, T., Englehardt, J.D., 2012. New Method for removal of hydrogen peroxide interference in the analysis of chemical Oxygen demand. *Environ. Sci. Technol.* 46, 2291–2298.
- Xu, B., Gao, N., Cheng, H., Hu, C.Y., Xia, S.J., Sun, X.F., Wang, X., Yang, S., 2009. Ametryn degradation by aqueous chlorine: Kinetics and reaction influences. *J. Hazard. Mater.* 169, 586–592.
- Xu, L., Wang, J., 2011. A heterogeneous Fenton-like system with nanoparticulate zerovalent iron for removal of 4-chloro-3-methyl phenol. *J. Hazard. Mater.* 186, 256–264.
- Xu, L., Wang, J., 2012. Fenton-like degradation of 2,4-dichlorophenol using Fe_3O_4 magnetic nanoparticles. *Appl. Catal., B* 123, 117–126.
- Xue, X., Hanna, K., Deng, N., 2009. Fenton-like oxidation of Rhodamine B in the presence of two types of iron (II, III) oxide. *J. Hazard. Mater.* 166 (1), 407–414.
- Yaping, Z., Jiangyong, H., 2008. Photo-Fenton degradation of 17β -estradiol in presence of α -FeOOHR and H_2O_2 . *Appl. Catal., B* 78 (3), 250–258.
- Yirsaw, B.D., Megharaj, M., Chen, Z., Naidu, R., 2016. Reduction of hexavalent chromium by green synthesized nano zero valent iron and process optimization using response surface methodology. *Envir. Technol. Innovation* 5, 136–147.
- Zhang, W., Gao, H., He, J., Yang, P., Wang, D., Maa, T., Xia, H., Xu, X., 2017. Removal of norfloxacin using coupled synthesized nanoscale zero-valent iron (nZVI) with H_2O_2 system: Optimization of operating conditions and degradation pathway. *Sep. Purif. Technol.* 172, 158–167.
- Zhang, Y., Klamerth, N., Messele, S.A., Chelme-Ayala, P., El-Din, M.G., 2016. Kinetics study on the degradation of a model naphthenic acid by ethylenediamine-N, N'-disuccinic acid-modified Fenton process. *J. Hazard. Mater.* 318, 371–378.
- Zhang, H., Li, Y.L., Wu, X.G., Zhang, Y.J., Zhang, D.B., 2010. application of response surface methodology to the treatment landfill leachate in a three-dimensional electrochemical reactor. *Waste Manage.* 30 (11), 2096–2102.
- Zhang, S.X., Zhao, X.L., Niu, H.Y., Shi, Y.L., Cai, Y.Q., Jiang, G.B., 2009. Superparamagnetic Fe_3O_4 nanoparticles as catalysts for the catalytic oxidation of phenolic and aniline compounds. *J. Hazard. Mater.* 167, 560–566.
- Zhou, D., Wu, F., Deng, N., Xiang, W., 2004. Photooxidation of bisphenol A (BPA) in water in the presence of ferric and carboxylate salts. *Water Res.* 38 (19), 4107–4116.
- Zinatizadeh, A.A.L., Mohamed, A.R., Abdullah, A.Z., Mashitah, M.D., Hasnain, Isa.M., Najafpour, G.D., 2006. Process modeling and analysis of palm oil mill effluent treatment in an up-flow anaerobic sludge mixed film bioreactor using response surface methodology (RSM). *Water Res.* 40, 3193–3208.
- Zuin, V.G., Schellin, M., Montero, L., Yariwake, J.H., Augusto, F., Popp, P., 2006. Comparison of stir bar sorptive extraction and membrane-assisted solvent extraction as enrichment techniques for the determination of pesticide and benzo-a-pyrene residues in Brazilian sugarcane juice. *J. Chromatogr. A.* 1114 (2), 180–187.